International Journal of Heat and Mass Transfer 52 (2009) 22–32

Contents lists available at ScienceDirect

International Journal of Heat and Mass Transfer

journal homepage: www.elsevier.com/locate/ijhmt

Transient two-dimensional model of frost formation on a fin-and-tube heat exchanger

Kristian Lenic *, Anica Trp, Bernard Frankovic

Faculty of Engineering, University of Rijeka, Vukovarska 58, HR-51000 Rijeka, Croatia

ARTICLE INFO

Article history:
Received 28 May 2008
Available online 23 July 2008

Keywords:
Frost formation
Fin-and-tube heat exchanger

ABSTRACT

In the paper, numerical and experimental analyses of heat and mass transfer during frost formation on a fin-and-tube heat exchanger have been presented. Modelling of the frost formation on cold surfaces placed in a humid air stream, requires a complex mathematical approach. A transient two-dimensional mathematical model of frost formation has been developed. The applied mathematical model has been defined using governing equations for the boundary layer that include air and frost sub-domains as well as a boundary condition on the air–frost interface. The mathematical model with initial and boundary conditions has been discretised according to the finite volume method and solved numerically using the SIMPLER algorithm for the velocity–pressure coupling. Results have shown that the frost layer formation significantly influences the heat transfer between air and fins. As a result of numerical calculations, time-wise frost thickness variations for different air humidities, temperatures and velocities have been presented. Using the developed mathematical model, the algorithm and the computer code, which have been experimentally validated, it is possible to predict a decrease of exchanged heat flux in the heat exchanger under frost growth conditions.

1. Introduction

The frost formation is a very common phenomenon in refrigeration that occurs when moist air near cold surfaces has been cooled below the freezing temperature of water. Thus, the frost layer grows on finned surfaces of the fin-and-tube heat exchanger used as an evaporation part of the heat pump working in the humid air. The frost layer is considered as a porous structure containing iced mesh including air gaps [1,2]. Whereas frost layer contains air pores with low thermal conductivity, the whole frost layer represents significant thermal resistance. A significant decrease of heat exchanger efficiency occurs due to augmented thermal resistance of the frost layer. Moreover, the free space between fins becomes smaller and hence, a higher pressure drop is generated causing a reduction of air flow. This has an effect on the space cooling quality and the service behaviour of the whole device [3]. The principal aim of the frost formation analysis is an estimation of exchanged heat flux under transient conditions of augmented thermal resistance.

During frosting process the frost layer exhibits different characteristics for each specific growth period [4]. When analysing frost growth phenomena, many authors divide the whole frost formation process into two [5] or regularly into three different periods [6]: crystal growth period, frost growth period and fully developed frost formation period.

For the prediction of frost growth, several models with various approximation degrees have been developed. The majority of models developed so far, can be classified into three groups. The first group represents a group of models which predict the variations of frost properties from the diffusion equation applied to the frost layer and then calculate the amount of heat and mass transfer in the frost layer using empirical correlations on the air side [5,7–10]. The second group of modelling methods gives some improvements and analyses the air flow using boundary layer equations and predicts the frost properties by using the empirical correlations [11]. The third group of models includes the modelling of frost growth using governing equations both for the air and the frost sides [2].

Many investigations are focused on specific geometries like parallel plates placed in a humid air stream in a laminar flow [12,13], vertical plate [14,15] and frost formation around cylinder [16]. In recent investigations it has been shown that the partial pressure of water vapour on frost layer surface is greater than partial pressure of water vapour for the temperature of frost layer surface, i.e. the air near the surface of frost layer is supersaturated [9,10].

During frost formation, not only the frost thickness changes, but also the frost density varies. The frost formation process depends on the water vapour transfer from air stream into the frost layer, on the diffusion rate of water vapour into the frost layer and on

* Corresponding author.
E-mail address: kristian.lenic@riteh.hr (K. Lenic).

0017-9310/$ - see front matter © 2008 Elsevier Ltd. All rights reserved.
doi:10.1016/j.ijheatmasstransfer.2008.06.005

Nomenclature

c_p	specific heat capacity under constant pressure, J kg^{-1} K^{-1}
D	diffusivity, m^2 s^{-1}
h	convective heat transfer coefficient, W m^{-2} K^{-1}
l	domain length, m
M	number of control volumes in horizontal direction
$\dot{m}$	water vapour mass flux, kg m^{-2} s^{-1}
$\dot{m}_a$	water vapour mass flux from air towards frost layer, kg m^{-2} s^{-1}
N	number of control volumes in vertical direction
p	pressure, Pa
q_{sub}	specific heat of sublimation, J kg^{-1}
S	supersaturation degree
s	distance between fins, m
T	temperature, °C
t	time, s
u_x	x-velocity component, m s^{-1}
u_y	y-velocity component, m s^{-1}
V	volume, m^3
W	specific thermal resistance, m^2 K W^{-1}
w	mass fraction of water vapour in air, kg kg^{-1}
x	coordinate, m
y	coordinate, m

Greek symbols

δ	layer thickness, m
ε	porosity
η	dynamic viscosity, Pa s
λ	thermal conductivity, W m^{-1} K^{-1}
ρ	density, kg m^{-3}
τ	tortuosity factor

Subscripts

a	air
cv	control volume
diff	related to diffusion into frost layer
eff	effective
fl	frost layer
fs	frost surface
i	ice
L	local value
s	fin surface
in	inlet
sat	saturated
v	water vapour
Δy	related to layer thickness increasing
0	initial value
∞	free air stream

the thermal conduction inside the layer. One part of the water vapour flux, which transfers from the air stream, has been deposited on the frost surface and it increases the frost thickness. The other part of water vapour flux enters the frost layer and thus increases its density. Accuracy of the determination of water mass flux entering the frost layer has crucial influence on the calculation accuracy of the frost layer growth rate. This indicates the necessity of further investigations in the field.

In the presented model, as a first improvement, calculations of air velocity, temperature and humidity fields have been performed allowing more exact description of heat and mass transfer on a frost–air interface. Some most recent acquirements from previous models have been introduced including prediction of supersaturated air at the air–frost interface according to [9,10]. Previous models, which used supersaturated air theory, have been solved only as one-dimensional mathematical models. The presented model gives an improvement because it has been defined and solved as transient and two-dimensional.

As afore-mentioned, during frost formation, three characteristic periods occur, Fig. 1. The crystal growth period is a relatively short period at the early stage of the frost formation process. Small water drops, which have been extracted from the air stream by condensation on cold fin surface, freeze almost instantaneously. These frozen water drops act as nuclei of further crystallisation. New ice crystals grow on these ice nuclei and spread out in all directions. It is very difficult to describe this period mathematically, although this initial period has a significant influence on further frost growth process. The influence of this period has been taken into account by choosing appropriate initial conditions.

The frost growth period, schematically shown in Fig. 1b, is characterised by a porous frost structure growing. The porous structure, composed of solid ice matrix filled with moist air gaps, is formed by branching and linking of new ice crystals. Thus, the frost layer surface becomes visible rugged due to new crystal formation on a surface. The transfer of water vapour from moist air towards frost layer leads to further growth and densification of the frost layer.

The fully developed frost formation period, Fig. 1c, occurs after the frost surface temperature has become equal to the temperature of ice melting. As frost layer grows, the thermal resistance of frost layer also grows, causing a surface temperature increasing. The water vapour condensing at the frost layer surface forms a thin liquid film that infuses into the frost layer and freezes in the deeper, colder parts of the frost layer. This causes an additional densification of the frost layer and augmentation of the frost layer thermal conductivity. The frost layer surface becomes smoother. Obviously, this happens only when inlet air temperature is above 0 °C. Subsequently, a cyclic process of condensing, melting, freezing and growth occurs until a thermal equilibrium of the whole frost layer has been obtained.

The presented mathematical model of frost growth applies to the frost growth period and the fully developed frost formation period, while the influence of crystal growth period is implemented into initial conditions.

2. Physical model and formulation

The fin-and-tube heat exchanger analysed in the paper is shown in Fig. 2. The refrigerant evaporates flowing through copper tubes and it cools the air which is flowing between thin aluminium fins. During this process, heat and mass transfer on a cooled surface occurs. This analysis deals only with physical processes on the air side of the heat exchanger assuming constant fin temperature.

The domain of calculation has been extracted from the physical model and it includes one-half of space between fins, as presented in Fig. 2b. The domain consists of two areas: subdomain of the humid air and subdomain of the frost layer, which are delimited by the air–frost interface. The lower boundary represents a cold fin surface, while at the top boundary a symmetrical boundary condition has been presumed.

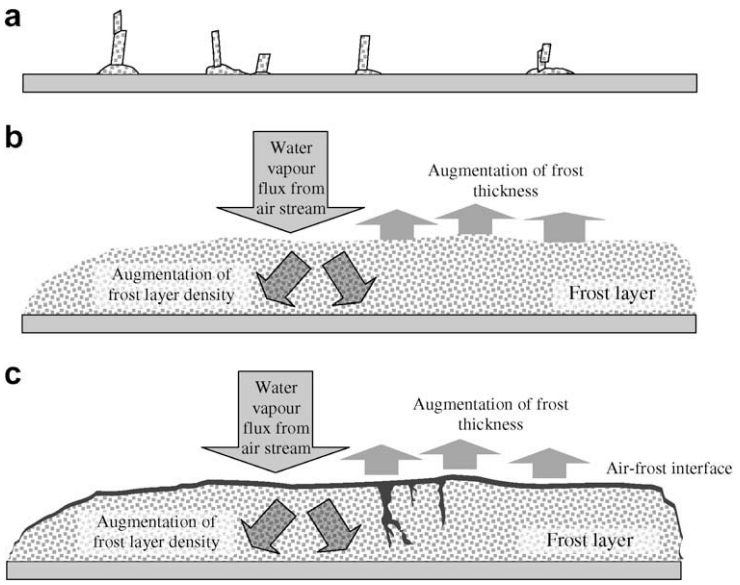

Fig. 1. Three characteristic periods during frost formation: (a) crystal growth period; (b) frost growth period; (c) fully developed frost formation period.

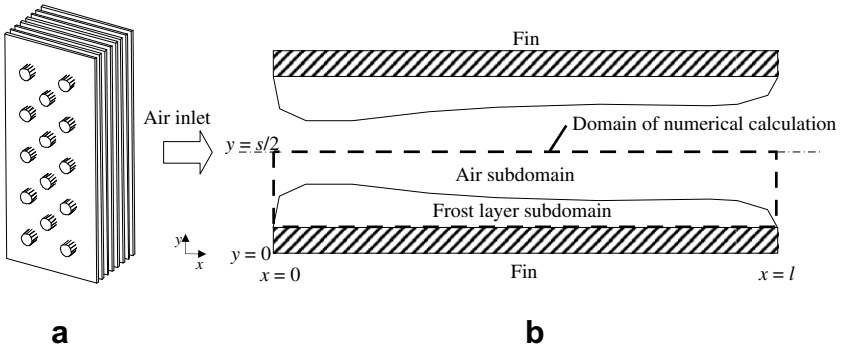

Fig. 2. Analysed fin-and-tube heat exchanger: (a) whole heat exchanger; (b) domain of numerical calculation between heat exchanger fins.

3. Mathematical model

The mathematical model, formulated in the two-dimensional Cartesian coordinate system, describes heat and mass transfer in the half space between heat exchanger fins. It has been assumed that the frost layer subdomain is a porous medium. The porosity of the frost layer is defined as follows:

$$\varepsilon = \frac{V_a}{V} = \frac{\rho_i - \rho_{fl}}{\rho_i - \rho_a}, \quad 0 \leqslant \varepsilon \leqslant 1 \tag{1}$$

Thus the density of frost layer can be calculated using

$$\rho_{fl} = \varepsilon \cdot \rho_a + (1 - \varepsilon) \cdot \rho_i \tag{2}$$

Following simplifications have been applied to define governing equations:

- humid air is considered as incompressible Newtonian fluid;
- fin surface temperature, as well as inlet air velocity, temperature and humidity are considered constant;
- the problem is symmetric;
- the thermal conductivity of frost layer is a function of density;
- the humid air at the air–frost interface is supersaturated.

3.1. Governing equations

Governing equations based on the above assumptions are defined for the dash framed computational domain shown in Fig. 2b.

Air subdomain

Continuity, momentum and energy equations as well as water vapour transport equation for the air subdomain are as follows:

$$\frac{\partial}{\partial x}(\rho_a u_x) + \frac{\partial}{\partial y}(\rho_a u_y) = 0 \tag{3}$$

$$\rho_a \frac{\partial u_x}{\partial t} + \rho_a \left(u_x \frac{\partial u_x}{\partial x} + u_y \frac{\partial u_x}{\partial y} \right) = -\frac{\partial p}{\partial x} + \eta \left(\frac{\partial^2 u_x}{\partial x^2} + \frac{\partial^2 u_x}{\partial y^2} \right) \tag{4}$$

$$\rho_a \frac{\partial u_y}{\partial t} + \rho_a \left(u_x \frac{\partial u_y}{\partial x} + u_y \frac{\partial u_y}{\partial y} \right) = -\frac{\partial p}{\partial y} + \eta \left(\frac{\partial^2 u_y}{\partial x^2} + \frac{\partial^2 u_y}{\partial y^2} \right) \tag{5}$$

$$\rho_a \frac{\partial T_a}{\partial t} + \rho_a \cdot \left(u_x \frac{\partial T_a}{\partial x} + u_y \frac{\partial T_a}{\partial y} \right) = \frac{\lambda_a}{c_{p,a}} \left(\frac{\partial^2 T_a}{\partial x^2} + \frac{\partial^2 T_a}{\partial y^2} \right) \tag{6}$$

$$\rho_a \frac{\partial w}{\partial t} + \rho_a \cdot \left(u_x \frac{\partial w}{\partial x} + u_y \frac{\partial w}{\partial y} \right) = \rho_a \cdot D \cdot \left(\frac{\partial^2 w}{\partial x^2} + \frac{\partial^2 w}{\partial y^2} \right) \tag{7}$$

Frost layer subdomain

For the frost layer subdomain energy equation and modified diffusion equation have been used.

$$\rho_{fl}\frac{\partial T_{fl}}{\partial t}=\frac{\partial}{\partial x}\left(\frac{\lambda_{fl}}{c_{p,fl}}\frac{\partial T_{fl}}{\partial x}\right)+\frac{\partial}{\partial y}\left(\frac{\lambda_{fl}}{c_{p,fl}}\frac{\partial T_{fl}}{\partial y}\right)+q_{sub}\frac{\partial \rho_{fl}}{\partial t} \tag{8}$$

$$\frac{\partial \rho_{fl}}{\partial t}=\frac{\partial}{\partial x}\left(D_{eff}\rho_a\frac{\partial(\rho_v/\rho_a)}{\partial x}\right)+\frac{\partial}{\partial y}\left(D_{eff}\rho_a\frac{\partial(\rho_v/\rho_a)}{\partial y}\right) \tag{9}$$

3.2. Initial and boundary conditions

3.2.1. Initial condition, $t = 0$

Air subdomain, $y_{fs} < y < s/2$

$$u_{x0}=0,\quad u_{y0}=0,\quad T_{a0}=T_{in},\quad w_0=w_{in} \tag{10}$$

Frost layer subdomain, $0 < y < y_{fs}$

$$T_{fl0}=T_s,\quad \rho_{fl0}=30\ \mathrm{kg/m^3} \tag{11}$$

It is assumed that the initial temperature of the frost layer is equal to the cold surface temperature. This assumption is valid if initial thickness is adequately small that thermal resistance of frost layer can be neglected compared to air side thermal resistance.

For the computation of the frost layer growth, it is required to predict the frost layer thickness and density at early stage of the frost formation. The influence of different initial frost layer thickness on calculation results has been already investigated [7]. Authors evaluated the effect of the initial value of the frost density on the frost growth rate by changing the value from 8 to 48 kg/m^3. They found that the frost thickness converged to the same value regardless the initial value of frost thickness, if it is chosen from the mentioned range. Based on their investigation, in this work the initial value of the frost density has been assumed to be 30 kg/m^3. The initial frost layer thickness is assumed to be 0.02 mm.

3.2.2. Boundary conditions, $t > 0$

$x = 0$, $0 < y < s/2$ – left (inlet) boundary

Air subdomain, $y_{fs} < y < s/2$

$$u_x=u_{in},\quad u_y=0,\quad T_a=T_{in},\quad w=w_{in} \tag{12}$$

Frost layer subdomain, $0 < y < y_{fs}$

$$\frac{\partial T_{fl}}{\partial x}=0,\quad \frac{\partial(\rho_v/\rho_a)}{\partial x}=0 \tag{13}$$

$0 < x < l$, $y = s/2$ – top boundary – symmetry plane

$$u_y=0,\quad \frac{\partial u_x}{\partial y}=0,\quad \frac{\partial T_a}{\partial y}=0,\quad \frac{\partial w}{\partial y}=0 \tag{14}$$

$x = l$, $0 < y < s/2$ – right (outlet) boundary

Air subdomain, $y_{fs} < y < s/2$

$$\frac{\partial u_x}{\partial x}=0,\quad \frac{\partial u_y}{\partial x}=0,\quad \frac{\partial T_a}{\partial x}=0,\quad \frac{\partial w}{\partial x}=0 \tag{15}$$

Frost layer subdomain, $0 < y < y_{fs}$

$$\frac{\partial T_{fl}}{\partial x}=0,\quad \frac{\partial(\rho_v/\rho_a)}{\partial x}=0 \tag{16}$$

$0 < x < l$, $y = 0$ – bottom boundary

$$T_{fl}=T_s,\quad \frac{\rho_v}{\rho_a}=\frac{\rho_v(T_s)}{\rho_a(T_s)} \tag{17}$$

3.2.3. Boundary condition on air frost interface $0 < x < l$, $y = y_{fs}$

Air velocity

$$u_x=0,\quad u_y=0 \tag{18}$$

Air humidity

Recent investigations have shown that the partial pressure of water vapour on frost layer surface is greater than partial pressure of water vapour for the temperature of frost layer surface, i.e. the air near the surface of frost layer is supersaturated [9,10]. Referent value for defining the supersaturation state is the supersaturation degree defined as follows:

$$S_v=\frac{p_v-p_{v,sat}}{p_{v,sat}} \tag{19}$$

Using the above definition, the mass fraction of water vapour in air on the air–frost interface is

$$w_{fs}=0.622\cdot\frac{(1+S_v)p_{v,sat}}{p_a-(1+S_v)p_{v,sat}} \tag{20}$$

Where the supersaturation degree is calculated using the following formula:

$$S=0.808\left(\frac{p_{v,\infty}}{p_{v,sat,\infty}}\right)\left(\frac{p_{v,sat,fs}}{p_{v,sat,\infty}}\right)^{-0{,}657}-1 \tag{21}$$

Temperature

The temperature of the frost layer surface is calculated using the following boundary condition for the energy equation:

$$\lambda_a\frac{\partial T_a}{\partial y}=\lambda_{fl}\frac{\partial T_{fl}}{\partial y}+q_{sub}\rho_{fl}\frac{dy_{fl}}{dt} \tag{22}$$

Density of new frost created at a frost surface

$$\frac{\partial \rho_{fl}}{\partial y}=0 \tag{23}$$

Frost surface moving

One part of the water vapour mass flux, which transfers from the air stream, has been deposited on the frost surface and increases the frost thickness. The other part of the water vapour flux enters the frost layer and increases its density. This can be expressed as follows:

$$\dot{m}_a=\dot{m}_{\Delta y}+\dot{m}_{diff} \tag{24}$$

The frost layer growth rate has been calculated using the total water vapour mass flux and the diffusive mass flux on a frost layer surface. The mass flux density of the water vapour which transfers from air to the frost layer surface is proportional to the gradient of air humidity:

$$\dot{m}_a=\rho_a\cdot D\cdot\frac{dw}{dy} \tag{25}$$

The mass flux density which increases the frost layer density absorbed by the frost layer is given by

$$\dot{m}_{diff}=-\rho_a\cdot D_{eff}\cdot\frac{d(\rho_v/\rho_a)}{dy} \tag{26}$$

The mass flux density responsible for the layer thickness growth is

$$\dot{m}_{\Delta y}=\rho_{fl}\frac{dy_{fl}}{dt}=\dot{m}_a-\dot{m}_{diff} \tag{27}$$

Thus, the frost layer growth rate is

$$\frac{dy_{fl}}{dt}=\frac{1}{\rho_{fl}}\dot{m}_{\Delta y}=\frac{1}{\rho_{fl}}(\dot{m}_a-\dot{m}_{dif}) \tag{28}$$

Physical properties of the frost layer

The effective thermal conductivity of the frost layer is related to the frost density. In this study, the following correlation proposed by Lee et al. [2] has been used:

$$\lambda_{fl}=0.132+3.13\cdot10^{-4}\rho_{fl}+1.6\cdot10^{-7}\rho_{fl}^2 \tag{29}$$

The specific heat of the frost layer is obtained from densities and specific heat capacities of ice and humid air, as well as density and porosity of the frost layer using

$$c_{p,fl} = \frac{1}{\rho_{fl}}\left[\rho_i(1-\varepsilon)c_{p,i} + \rho_a \varepsilon c_{p,a}\right] \quad (30)$$

The effective diffusion coefficient, as proposed by Na and Weeb [9,10], has been calculated using

$$D_{eff} = D \cdot \varepsilon \cdot \tau = D \cdot \varepsilon \cdot \frac{1+\varepsilon}{2} \quad (31)$$

Where the tortuosity factor has been defined as follows:

$$\tau = \frac{1+\varepsilon}{2} \quad (32)$$

4. Numerical calculations

The governing equations are discretised using control volume method. Staggered grids for velocity components have been used to avoid physically unrealistic pressure field in the air subdomain. The convection-diffusion terms have been discretised using power-law scheme and the resulting set of linearised discretisation equations have been solved using an iterative procedure. A fully implicit method has been used for time-stepping treatment. For the velocity–pressure coupling the SIMPLER algorithm has been applied [17,18]. Physical property data have been stored in a separate input files. The algorithm has been implemented in a self-written FORTRAN code and solved on a personal computer.

Detailed description of the numerical approach has been given in [19].

5. Experimental validation

The physical validity of the computational model has been studied by comparison of numerical results with experimental data. Inlet conditions during the experimental investigation have been used as input data in numerical simulations.

The experimental investigations have been carried out in a test unit containing semi-open air tunnel, Fig. 3. Air tunnel has been built of aluminium sheet with radial fan mounted at the inlet and the test section at the outlet side. The test section consisted of a vertically positioned aluminium plate cooled by direct evaporation of the refrigerant. The whole air tunnel has been placed in the chamber with controlled temperature and humidity conditions.

The experimental measurements have been carried out for different inlet air temperatures in the range 19–23 °C and different humidity conditions in the range 37–60% of relative humidity. In order to measure the temperature distribution, eight K-type thermocouples (field 4 × 2) have been placed on the cooled aluminium plate positioned as shown in Fig. 3. Additional temperature, relative humidity and velocity sensor have been placed at the inlet of the test section. All thermocouples have been connected to a data acquisition system. The Labview commercial software has been used to process and record data in a database format using the personal computer. The temperature data measured by thermocouples have been recorded every 4 s within total testing time of 6 h for each different air condition set.

The numerical model has been validated by simulating the experimental conditions. Therefore numerical calculations have been performed for a grid size of 300 (longitudinal) and 100 (transversal) nodes. The domain has been discretised in rectangular control volumes with 0.4 and 0.1 mm side length. In Fig. 4, time-wise temperature variations at thermocouples' locations Tc1–Tc4 are shown for both experiment and simulation under different conditions. Time-wise frost layer thickness variations with comparison of numerical and experimental data are also shown in Fig. 4. The comparison between numerical predictions and experimental data for frost layer growth in a humid air stream shows a satisfactory good agreement regarding trends of analysed variables. The results obtained pointed out that the developed numerical procedure could be efficiently used to simulate the physical process of the frost layer formation.

6. Calculation results

After the validation of the mathematical model and a computer code, numerical analyses have been performed for a fin-and-tube heat exchanger with the geometry characteristics presented in Table 1.

A set of numerical calculations has been performed in order to evaluate the influence of inlet air velocity, temperature and humidity on the frost growth rate. Numerical analysis has been carried out for different inlet air velocities, temperatures and humidities. The sets of conditions used for numerical calculations are shown in Table 2. All calculations have been performed for constant fin surface temperature of 12 °C. Inlet air velocities varied from 1 to 1.4 m/s, while inlet air temperatures were in the range from 0 to 12 °C. Water mass fraction in the air varied from 0.001 to 0.008 kg/kg corresponding to relative humidity from 20% to 90% regarding related temperatures. As results of numerical analysis, velocity and temperature fields as well as distributions of frost thickness have been obtained.

6.1. Frost layer growth

Frost layer thickness and velocity field time variations for two cases of different air humidities and different air temperatures

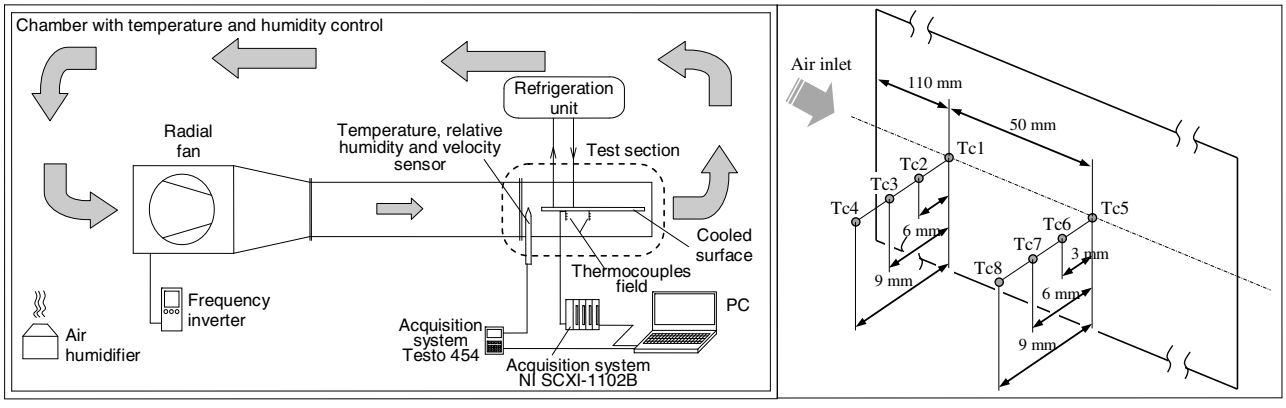

Fig. 3. Experimental setup and nomenclature of thermocouples.

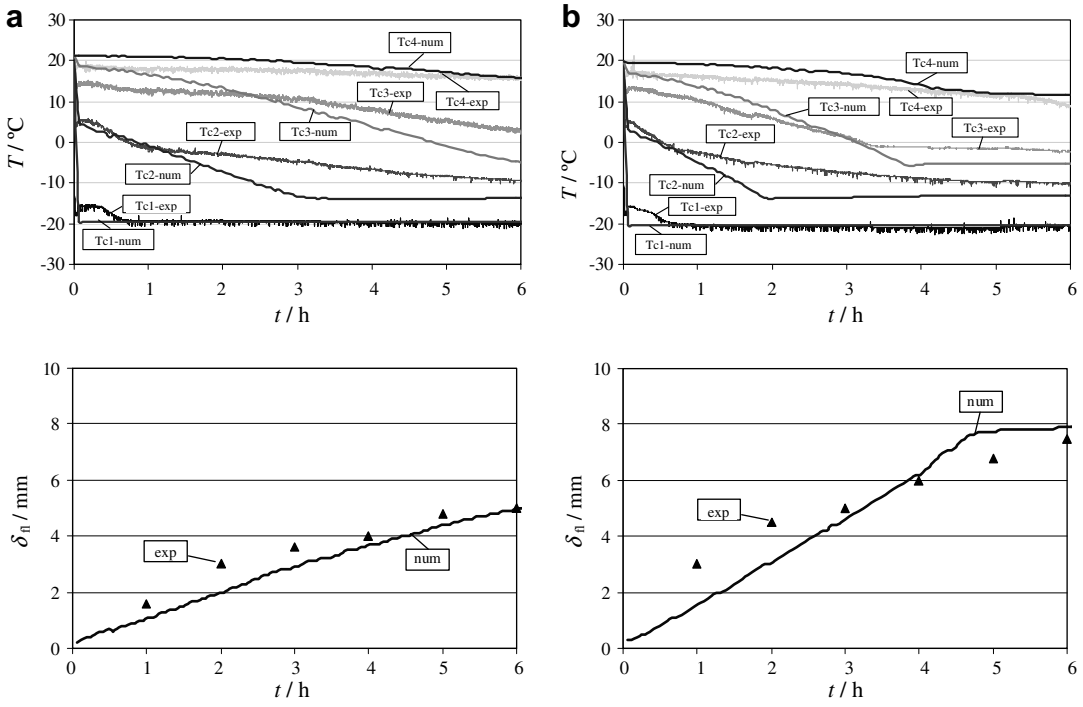

Fig. 4. Time-wise temperature variations and frost layer thickness variations at location $x = 120$ mm – comparison of experimental and numerical values: (a) $u_{x,in} = 0.6$ m/s, $T_{a,in} = 21.4$ °C, $w_{in} = 0.0062$ kg/kg, $T_s = -19.5$ °C; (b) $u_{x,in} = 0.6$ m/s, $T_{a,in} = 19.8$ °C, $w_{in} = 0.0082$ kg/kg, $T_s = -20.5$ °C.

Table 1
Geometry characteristics of analysed fin-and-tube heat exchanger

Fin thickness, m	0.001
Space between fins, m	0.010
Fin width, m	0.048
Longitudinal pipe distance, m	0.016
Transversal pipe distance, m	0.014
Outer pipe diameter, m	0.01
Inside pipe diameter, m	0.008

have been shown in Fig. 5. The frost layer, growing under A1 test conditions, has a moderately uniform thickness. The frost layer surface becomes rough, what is attributed to the second phase of the frost formation process. At the inlet part (left side of the calculation domain), the frost layer is slightly thicker. Here, the boundary layer has not been completely developed and the frost layer surface is in contact with the inlet air stream and the inlet humidity. Downstream, a little distant from the inlet boundary, the boundary layer in the air stream is well developed what can be seen from a parabolic distribution of the velocity in transversal direction. In the central symmetric plane ($y = s/2 = 5$ mm), maximal velocities have been obtained and near the air–frost interface air velocities become smaller. This has a significant influence on a convective heat transfer on the air–frost interface.

During first 3 h of the frost formation under A1 conditions, only the first and the second phase in the frost formation process occur. The third phase, i.e. the fully developed frost formation period, has not been reached yet. During A3 test conditions with higher inlet air humidity, more intensive frost formation occurs in comparison with the case under A1 test conditions with lower inlet air humidity. The growth of frost layer is more intensive under higher air humidity because of the higher gradient of air humidity near the frost surface in the boundary layer. The influence of the air humidity on the frost layer growth rate is also very significant.

In the beginning, the frost formation process is more intensive at the inlet part of the heat exchanger. The second phase of the frost formation process takes place on the whole domain. As the frost layer grows, the gradually increasing of the frost surface temperature occurs due to augmentation of the frost heat transfer resistance. After frost surface temperature has reached 0 °C, a thin water film forms on a frost layer surface. It soaks into the frost layer and freezes in colder areas of the layer. The frost layer surface becomes smoother. Thus, the third phase of frost layer formation occurs. It occurs first at the inlet parts of the domain. The area in-

Table 2
Overview of numerical analysis conditions

Test condition identifier	Temperature of fin surface T_s (°C)	Inlet air temperature $T_{a,in}$ (°C)	Inlet air velocity $u_{x,in}$ (m/s)	Inlet air humidity w_{in} (kg/kg)
A1	−12	12	1	0.002
A2	−12	12	1	0.004
A3	−12	12	1	0.006
A4	−12	12	1	0.008
B1	−12	5	1	0.001
B2	−12	5	1	0.002
B3	−12	5	1	0.004
C1	−12	0	1	0.001
C2	−12	0	1	0.002
D1	−12	12	1.2	0.004
D2	−12	12	1.4	0.004

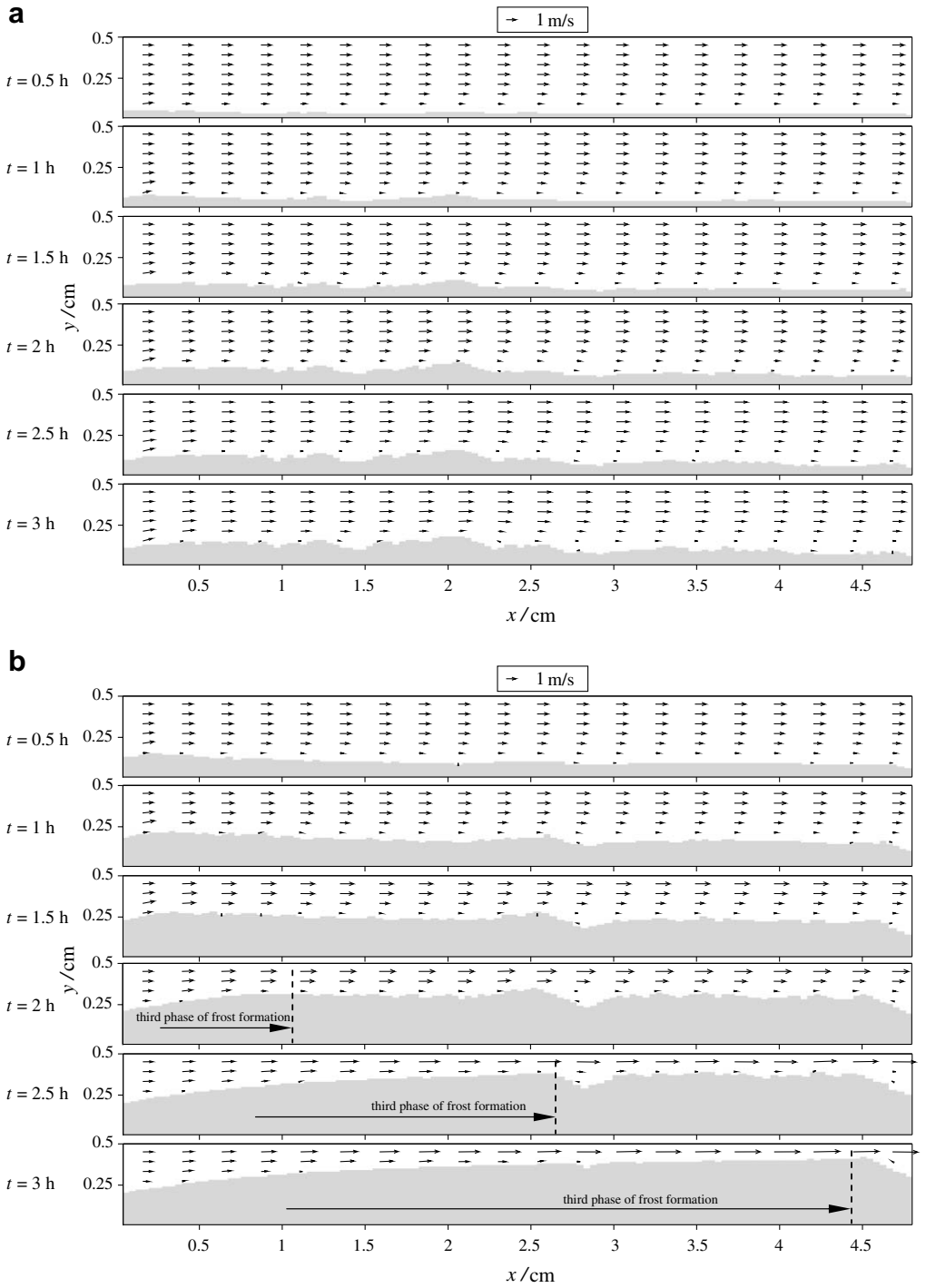

Fig. 5. Frost layer thickness and velocity field time variations: (a) A1 test conditions ($u_{x,in}$ = 1 m/s, $T_{a,in}$ = 12 °C, w_{in} = 0.002 kg/kg, T_s = −12 °C); (b) A3 test conditions ($u_{x,in}$ = 1 m/s, $T_{a,in}$ = 12 °C, w_{in} = 0.006 kg/kg, T_s = −12 °C).

volved in the third phase of frost formation extends then to the right, towards the outlet boundary. At some stages, both the second and the third phase of the frost formation process occur simultaneously on different sides of the domain.

6.2. Temperature distributions

Cooling of the air stream is caused by heat transfer from the air towards frost layer, fins and finally towards refrigerant medium which flows and evaporates inside the heat exchanger tubes. The average temperature at transversal cross-section becomes lower from the inlet to the outlet. As frost layer grows, the conditions of heat transfer significantly change due to the variation of the heat transfer resistance. During regular operation the frost layer becomes thicker and the frost surface temperature becomes higher due to increased thermal resistance. Transversal distributions of temperatures at position x = 15 mm for different times of frost formation are shown in Fig. 6. It can be seen that temperature distributions inside the frost layer are linear. As opposite in the air boundary layer temperature distributions are non-linear. The point, at which curve of temperature distribution changes its flow, represents the temperature of the frost layer surface. Temperatures of the frost

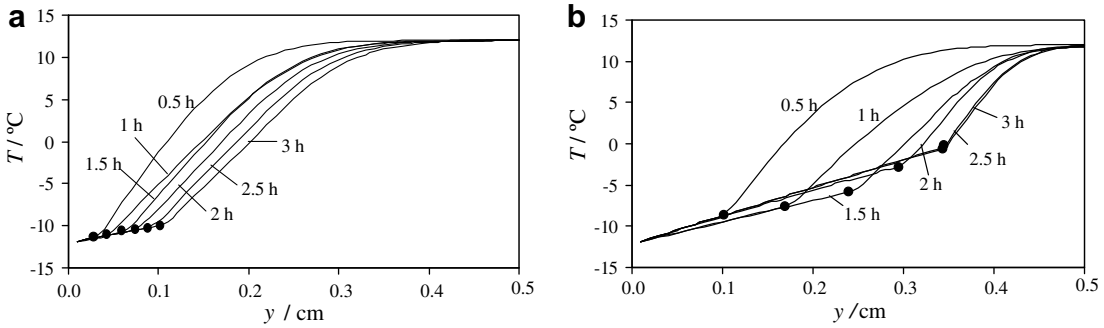

Fig. 6. Transversal distributions of temperatures for different times of frost formation at $x = 15$ mm: (a) A1 test conditions ($u_{x,in} = 1$ m/s, $T_{a,in} = 12$ °C, $w_{in} = 0.002$ kg/kg, $T_s = -12$ °C); (b) A3 test conditions ($u_{x,in} = 1$ m/s, $T_{a,in} = 12$ °C, $w_{in} = 0.006$ kg/kg, $T_s = -12$ °C).

layer surface at 0.5 h time intervals have been marked with black dots. It can be noticed that under the test conditions A3 (Fig. 6b), the temperatures of the frost layer surface are growing during the second phase of frost layer formation process. After reaching the third phase of frost formation process, the thermal equilibrium has been reached, and temperatures do not change significantly (after 2.5 h). Under the test conditions A1 (Fig. 6a), the third phase of frost formation have not been reached during first 3 h, thus the temperature of frost surfaces rises continuously. Temperature fields time variations for the related test conditions are shown in Fig. 7.

6.3. Air humidity distributions

The growth rate of the frost layer mostly depends on the mass flux of the water vapour from moist air towards air–frost interface. The mass flux is proportional to the gradient of air humidity near the air–frost interface. Due to the mass transfer towards the frost layer, the average amount of water in the air decreases from inlet to outlet boundary. Transversal distributions of the water mass fraction in moist air for different times of frost formation period at position $x = 15$ mm are shown in Fig. 8. Mass fraction of water vapour in moist air is lower near air–frost interface than in the central plane of the air stream.

During A3 test conditions, the gradient of air humidity in the transversal cross-section is higher than during A1 test conditions. This causes a more intensive transfer of the water vapour towards the frost layer.

6.4. Convective heat transfer coefficient at the air–frost interface

Longitudinal distributions of local convective heat transfer coefficients on the frost layer surface are shown in Fig. 9. In case of lower inlet humidity, the value of local convective heat transfer coefficients ranges from 4 to 20 $W\,m^{-2}\,K^{-1}$. The convective heat transfer is more intensive at the inlet part, due to the higher difference between the air temperature and the frost surface temperature. Because of decreasing of the temperature difference towards the outlet boundary, local convective heat transfer coefficients decrease in the air flow direction.

In case of higher inlet air humidity (A3 test conditions) the value of local convective heat transfer coefficients ranges from 5 to 20 $W\,m^{-2}\,K^{-1}$, tending to increase during time. Intensive frost layer growth causes reduction of free space between heat exchanger fins. This leads to the increase of air velocity and to intensification of the convective heat transfer. The just mentioned moderate increasing of the convective heat transfer coefficient does not have significant influence on the overall heat transfer between air and fins. The influence of increased thermal resistance due to thicker frost layer is more significant than the influence of increased convective heat transfer on air–frost interface.

6.5. Conductivity of the frost layer

The most significant undesirable consequence of the frost layer formation on a fin-and-tube heat exchanger is an augmentation of the thermal resistance. This affects the exchanged heat flux and in consequence results with decrease of the heat exchanger efficiency. In order to determine some changes in the frost layer heat resistance, it is necessary to calculate the mean conductivity of the whole frost layer for each time step. Because of the heterogeneity of the frost layer and different mechanisms of frost formation in different phases of the frost formation process, areas of different porosities i.e. densities have been formed. This has been manifested by irregular distribution of local conductivities of the frost layer. The local conductivity of the frost layer has been calculated using

$$\lambda_L = \frac{N}{\sum_{cv=1}^{N} \frac{1}{\lambda_{cv}}} \tag{33}$$

Where N corresponds to the thickness of the frost layer expressed as a number of control volumes with height Δy, while λ_{cv} represents the coefficient of thermal conductivity for individual control volume.

The local specific thermal resistance is a ratio of the local frost layer thickness and local thermal conductivity as it is represented by the following formula:

$$W_L = \frac{N \cdot \Delta y}{\lambda_L} = \Delta y \cdot \sum_{cv=1}^{N} \frac{1}{\lambda_{cv}} \tag{34}$$

The average value of specific thermal resistance of the whole frost layer has been calculated using

$$\overline{W}_{fl} = \frac{\sum_{k=1}^{M} W_{L,k}}{M} \tag{35}$$

The thermal resistance of a frost layer grows as the frost layer becomes thicker. Growth intensity of thermal resistance corresponds to the dynamics of the frost layer formation.

Initially, the thermal resistance grows faster, but when the third phase of frost formation has been reached, the growing of the thermal resistance slows down as the frost layer also grows slower.

Distributions of local thermal conductivity and local specific thermal resistance of the frost layer for different times of frost formation are shown in Fig. 10.

From the distribution of local values it can be noticed that the conductivity of frost layer is higher at the inlet part of a domain while the appropriate thermal resistance is relatively low. Higher values of thermal conductivity at the inlet part are the result of higher frost density, since the third phase of frost formation occurs in a short time. The third phase of frost formation is characterised by the increasing of frost density due to penetration of the liquid water into the frost layer. Water freezes in the deeper, colder parts

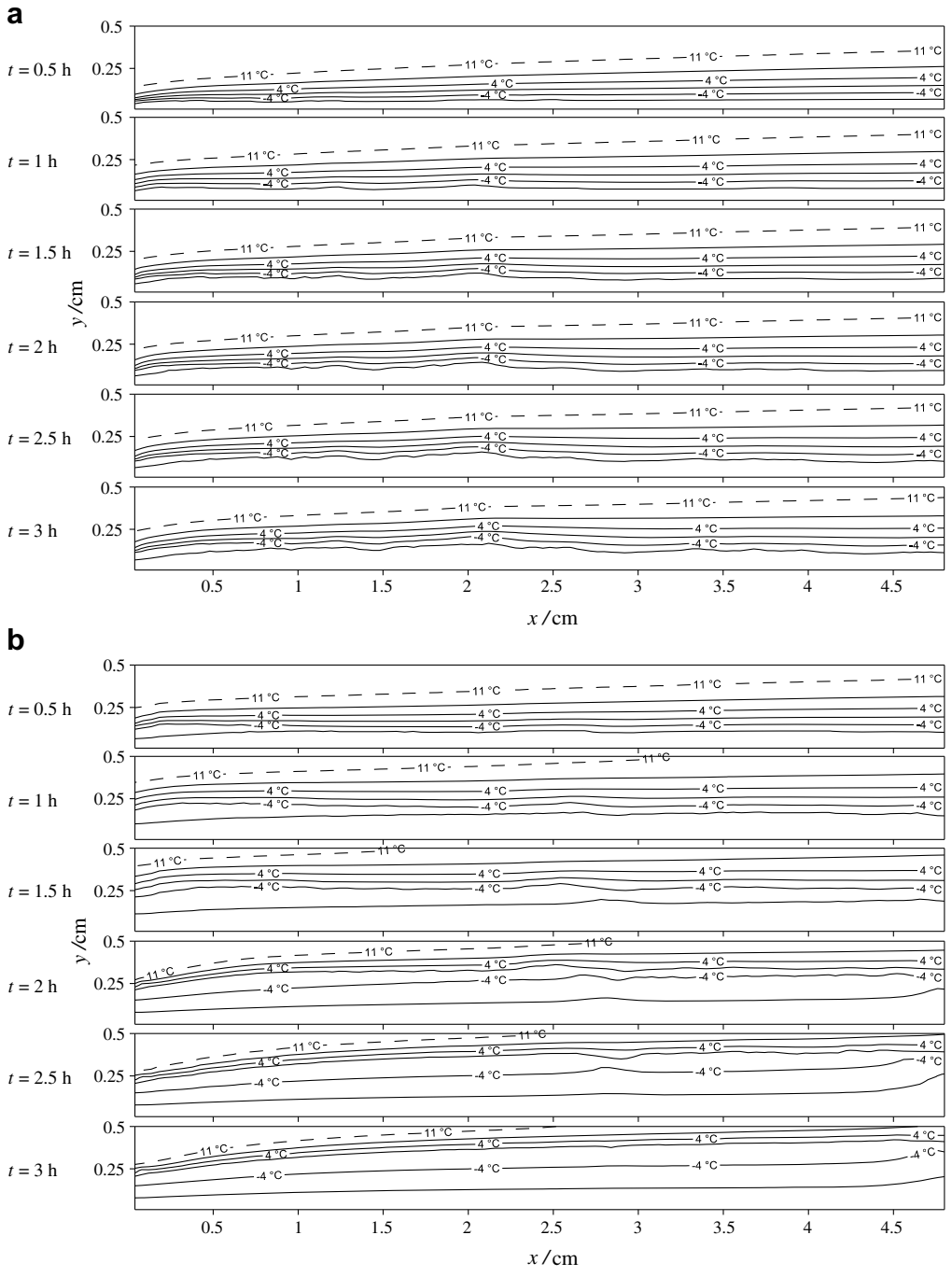

Fig. 7. Temperature field time variations: (a) A1 test conditions ($u_{x,in}$ = 1 m/s, $T_{a,in}$ = 12 °C, w_{in} = 0.002 kg/kg, T_s = −12 °C); (b) A3 test conditions ($u_{x,in}$ = 1 m/s, $T_{a,in}$ = 12 °C, w_{in} = 0.006 kg/kg, T_s = −12 °C) – isotherms −8, −4, 0, 4, 8 and 11 °C.

of the frost layer and it increases the frost density. The porosity of frost becomes lower and frost layer contains more ice crystals which have higher thermal conductivity than air gaps. This causes the increasing of frost layer thermal conductivity. Overall heat conductivity of the frost layer grows during frost formation process.

During the frost formation process one part of water vapour flux condenses and solidifies on a frost surfaces and consequently increases the frost layer thickness. The other part of water vapour flux penetrates by diffusion into frost layer and increases the frost density. The increasing of frost density, caused by water vapour diffusion, leads to the augmentation of thermal conductivity and finally to the reduction of the thermal resistance of the frost layer. Simultaneously, the increasing of the frost layer thickness causes the increasing of thermal resistance. The impact of the increased thickness is more significant than the impact of the increased thermal conductivity. As a result of both effects, the thermal resistance of frost layer increases during frost formation period.

6.6. Influence of the air velocity, humidity and temperature on frost growth

The changing of the thermal resistance of the frost layer has substantial influence on the exchanged heat flux in a heat exchanger which operates in conditions of frost layer formation. Therefore, the analyses of operating conditions' influence on frost layer growth rate have been carried out. As an authentic indicator for

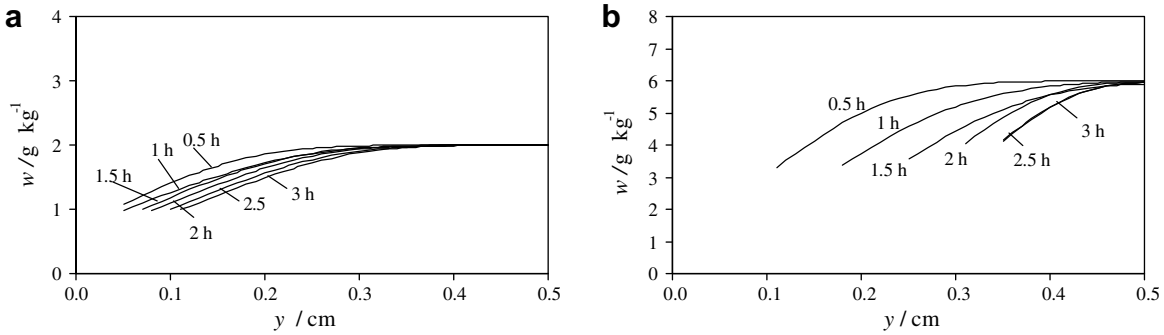

Fig. 8. Transversal distributions of air humidities for different times of frost formation at $x = 15$ mm: (a) A1 test conditions ($u_{x,in} = 1$ m/s, $T_{a,in} = 12$ °C, $w_{in} = 0.002$ kg/kg, $T_s = -12$ °C); (b) A3 test conditions ($u_{x,in} = 1$ m/s, $T_{a,in} = 12$ °C, $w_{in} = 0.006$ kg/kg, $T_s = -12$ °C).

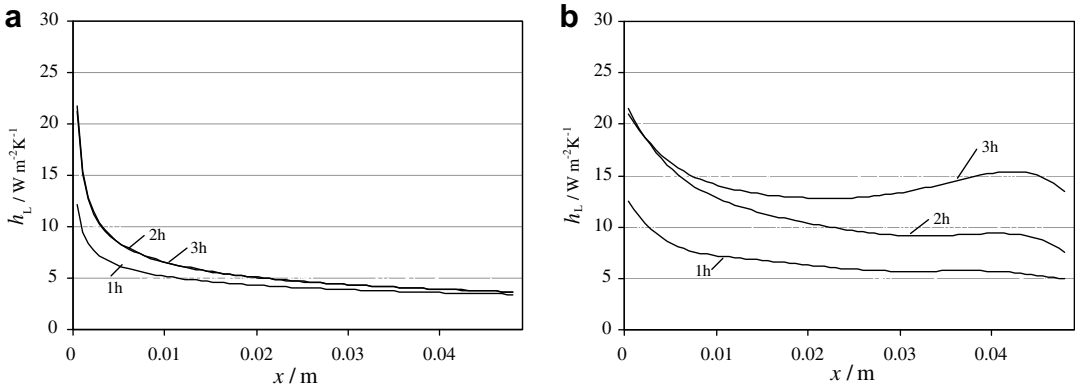

Fig. 9. Longitudinal distributions of local convective heat transfer coefficients on the frost layer surface: (a) A1 test conditions ($u_{x,in} = 1$ m/s, $T_{a,in} = 12$ °C, $w_{in} = 0.002$ kg/kg, $T_s = -12$ °C); (b) A3 test conditions ($u_{x,in} = 1$ m/s, $T_{a,in} = 12$ °C, $w_{in} = 0.006$ kg/kg, $T_s = -12$ °C).

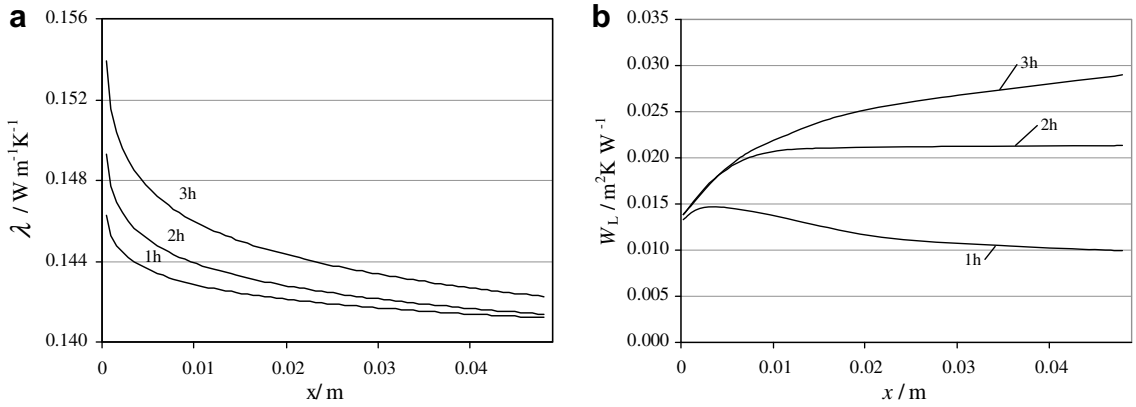

Fig. 10. Longitudinal distributions under A3 test conditions for different times of frost formation: (a) local thermal conductivity of the frost layer; (b) local specific thermal resistance of the frost layer.

monitoring the frost growth an average layer thickness has been used. The average layer thickness has been defined as follows:

$$\delta_{fl} = \frac{\sum_{k=1}^{M} \delta_{L,k}}{M} \tag{36}$$

The time-wise average frost thickness variation for different inlet velocities has been shown in Fig. 11a. When higher inlet air velocities are applied, the frost layer grows faster, although the impact of the air velocity on frost growth is minimal for the analysed velocity range. Faster development of the frost layer has been caused by increased gradient of air humidity near the air–frost interface, when higher air velocity has been applied. This higher air humidity gradient results with higher water vapour flux directed towards the frost layer. As a result of numerical analyses, which have been carried out for different inlet air humidities, a relation between inlet air humidity and frost growth rate has been obtained. Time variations of average frost layer thickness for different air humidities have been shown in Fig. 11b. Frost layer growth is more intensive under higher air humidities because of higher gradient of air humidity near the frost surface in the boundary layer. This influence of air humidity on the frost layer growth rate is substantial. Time variations of average frost layer thickness for different air inlet temperatures and un-

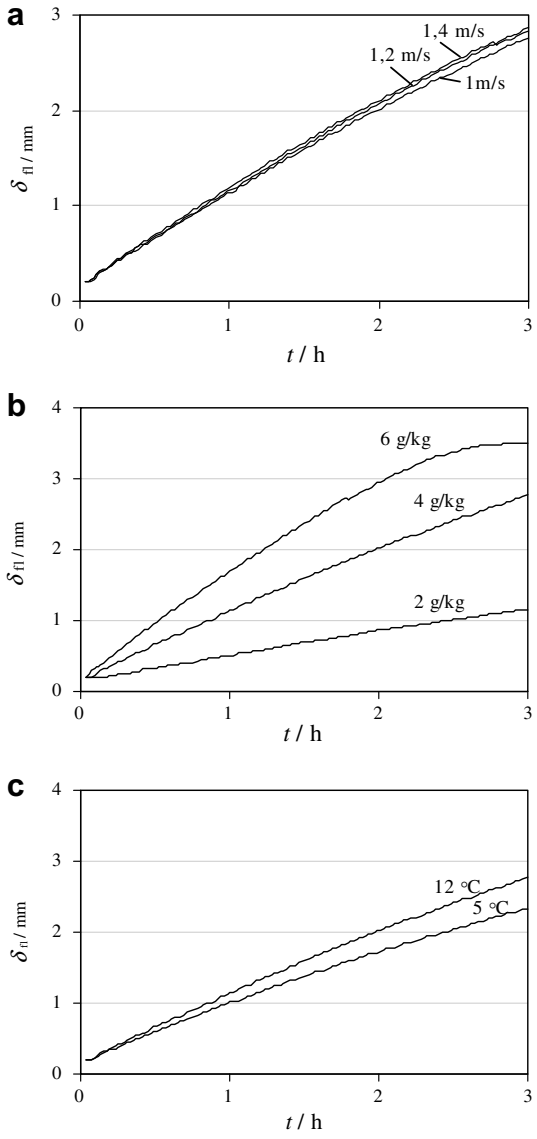

Fig. 11. Time-wise average frost thickness variation: (a) for different inlet velocities ($T_{a,in}$ = 12 °C, w_{in} = 0.004 kg/kg, T_s = −12 °C); (b) for different air humidities ($u_{x,in}$ = 1 m/s, $T_{a,in}$ = 12 °C, T_s = −12 °C); (c) for different air inlet temperatures ($u_{x,in}$ = 1 m/s, w_{in} = 0.004 kg/kg, T_s = −12 °C).

der constant water mass fraction in the air of 0.004 kg/kg are shown in Fig. 11c. Applying the lower air temperature, the frost layer formation is slower than in case when higher inlet air temperatures have been used. However, the influence of air temperature is not so significant.

7. Conclusions

Investigations described in this paper have included numerical and experimental analyses of heat and mass transfer during the frost formation on a fin-and-tube heat exchanger. The developed mathematical model enables the calculation of velocity, temperature and humidity fields around and inside the frost layer. Results have shown that phenomena of frost formation on a cold surfaces placed in a humid air stream requires a complex mathematical approach. The numerical analysis should take into account the porous nature of the frost layer and appropriate physical proprieties must be calculated. During the frost layer growth, an increasing of the frost density occurs and influences the thermal conductivity of the frost layer and finally influences the exchanged heat flux. Frost layer formation significantly influences the heat transfer from air to refrigerant which evaporates inside the heat exchanger pipes. It can be concluded that the frost layer growth is faster when the inlet air humidity and inlet air temperature are higher, while the influence of inlet air velocity on the frost growth rate can bee neglected. Using the developed mathematical model, algorithm and computer code, which have been experimentally validated, it is possible to predict a decrease of the exchanged heat flux in a heat exchanger under the frost growth conditions.

Acknowledgements

This research has been performed as a part of the scientific project *Research and Development of Renewable Energy Components and Systems*, supported by the Ministry of Science, Education and Sports of the Republic of Croatia.

References

[1] Y.X. Tao, R.W. Besant, K.S. Reykallah, A mathematical model for predicting the densification and growth of frost on a flat plate, Int. J. Heat Mass Transfer 36 (1993) 353–363.
[2] K. Lee, S. Jhee, D. Yang, Prediction of the frost formation on a cold flat surface, Int. J. Heat Mass Transfer 46 (2003) 3789–3796.
[3] C.T. Sanders, The Influence of Frost Formation and Defrosting on the Performance of Air Coolers, Ph.D. Thesis, Delft Technical University, Delft, 1974.
[4] Y. Hayarishi, A. Aoki, S. Adachi, K. Hori, Study of frost properties correlating with frost formation types, J. Heat Transfer 99 (1977) 239–245.
[5] K.S. Lee, W.S. Kim, T.H. Lee, A one-dimensional model for frost formation on a cold surface, Int. J. Heat Mass Transfer 40 (1997) 4359–4365.
[6] R. Le Gall, J.M. Grillot, C. Jallut, Modelling of frost growth and densification, Int. J. Heat Mass Transfer 40 (1997) 3177–3187.
[7] B.W. Jones, J.D. Parker, Frost formation with varying environmental parameters, J. Heat Transfer 97 (1975) 255–259.
[8] A.Z. Sahin, An analytical study of frost nucleation and growth during the crystal growth period, Heat Mass Transfer 30 (1995) 321–330.
[9] B. Na, R.L. Weeb, New model for frost growth rate, Int. J. Heat Mass Transfer 47 (2004) 925–936.
[10] B. Na, R.L. Weeb, Mass transfer on and within a frost layer, Int. J. Heat Mass Transfer 47 (2004) 899–911.
[11] S.A. Sherif, S.P. Raju, M.M. Padki, A.B. Chan, A semi-empirical transient method for modelling frost formation on a flat plate, ASME Heat Transfer Div. 139 (1990) 15–23.
[12] A. Lüer, H. Beer, Frost deposition in a parallel plate channel under laminar flow conditions, Int. J. Therm. Sci. 39 (2000) 85–95.
[13] K.A.R. Ismail, C.S. Salinas, Modelling of frost formation over parallel cold plates, Int. J. Refrig. 22 (1999) 425–441.
[14] M. Fossa, G. Tanda, Study of free convection frost formation on a vertical plate, Exp. Therm. Fluid Sci. 26 (2002) 661–668.
[15] Y.B. Lee, S.T. Ro, Frost formation on a vertical plate in simultaneously developing flow, Exp. Therm. Fluid Sci. 26 (2002) 939–945.
[16] K.A.R. Ismail, C. Salinas, M.M. Goncalves, Frost growth around a cylinder in a wet air stream, Int. J. Refrig. 20 (1997) 106–119.
[17] S.V. Patankar, Numerical Heat Transfer and Fluid Flow, Hemisphere Publishing Corporation Taylor & Francis Group, New York, 1980.
[18] H.K. Versteeg, W. Malalasekera, An Introduction to Computational Fluid Dynamics: The Finite Volume Method, Longman Scientific and Technical, Essex, England, 1995.
[19] K. Lenic, Analysis of Heat and Mass Transfer During Frost Formation on Fin-and-Tube Heat Exchangers, Ph.D. thesis, Faculty of Engineering University of Rijeka, Rijeka, Croatia, 2006 (in Croatian).